Chemical Science

ROYAL SOCIETY OF CHEMISTRY

EDGE ARTICLE

View Article Online
View Journal | View Issue

Cite this: *Chem. Sci.*, 2025, **16**, 20906

All publication charges for this article have been paid for by the Royal Society of Chemistry

Received 12th August 2025
Accepted 30th September 2025

DOI: 10.1039/d5sc06142c

rsc.li/chemical-science

Click-assembled N-graphene–C_{60} hybrids for ultrafast electron transfer

Luis M. Arellano, [a] Habtom B. Gobeze,[b] Youngwoo Jang,[b] María J. Gómez-Escalonilla, *[a] Paul A. Karr,[c] Francis D'Souza *[b] and Fernando Langa *[a]

A novel donor–acceptor hybrid derived from N-doped graphene (**NG**) and an electron acceptor, C_{60}, has been newly synthesized using click chemistry and characterized by a suite of physico–chemical techniques. The usage of click chemistry resulted in a relatively high degree of functionalization. Due to the presence of two C_{12} alkyl chains on the fulleropyrrolidine moiety, the **NG-C_{60}** hybrid was found to be relatively soluble in most organic solvents, facilitating both spectroscopic and electrochemical characterization. Fluorescence studies revealed quenching of the fulleropyrrolidine emission, indicating the occurrence of excited-state events. While DFT studies provided insights into the geometry and localization of the frontier orbitals, the TD-DFT studies performed at the B3LYP/6-311G(d,p) level suggested the possibility of excited-state charge transfer from several excited states. Subsequent femtosecond transient absorption studies performed in DMF confirmed electron transfer, wherein the material could be characterized. The charge transfer state persisted for approximately 12 ps before populating the low-lying $^3C_{60}$*, highlighting the material's potential for light energy harvesting applications.

Introduction

The increasing global demand for sustainable energy solutions has intensified research into materials capable of harvesting and converting solar energy with high efficiency. Among the various strategies explored, the design of donor–acceptor (D–A) systems that facilitate photoinduced electron transfer (ET) has emerged as a particularly promising approach.[1,2] These systems emulate key aspects of natural photosynthesis, where efficient charge separation and migration are essential for energy conversion.[3] Fullerenes, especially C_{60}, have long been recognized as prototypical zero-dimensional electron acceptors due to their high electron affinity, low reorganization energy, and excellent photostability.[4] Their integration into artificial photosynthetic assemblies has led to significant advances in the development of photovoltaic and photocatalytic devices.[5–12]

In parallel, graphene and its derivatives have acquired considerable attention as potential electron donors in D–A systems.[5,13–20] While pristine graphene is a zero-band-gap material with limited reactivity, heteroatom doping—particularly with nitrogen—introduces localized electronic states and reactive sites that enhance both its chemical versatility and electronic properties.[21–23] Nitrogen-doped graphene (**NG**) exhibits improved conductivity, tunable band structure, and enhanced interaction with electron-accepting species, making it an ideal platform for constructing hybrid nanomaterials.[24,25]

A few years ago, we reported the first example of nitrogen-doped graphene (**NG**) functionalization *via* derivatization at the heteroatom.[26] Building on this strategy, we subsequently achieved the covalent attachment of C_{60} to **NG**, thereby constructing a novel donor–acceptor hybrid.[27] However, the synthetic approach employed in that study was relatively inefficient, yielding only moderate product quantities and requiring extended reaction times. To overcome these limitations, the present work introduces a new and more effective method for linking C_{60} to **NG**, employing the well-established copper-catalyzed azide–alkyne cycloaddition (click chemistry). This approach enables higher functionalization efficiency, improved yields, and reduced reaction times, facilitating the development of advanced carbon-based donor–acceptor systems.[28] As demonstrated in this study, the use of click chemistry enabled significantly improved reaction yields, reduced reaction times, and a higher degree of functionalization. Additionally, femtosecond transient spectroscopy revealed ultrafast charge separation, highlighting the novelty of this work. Following the successful synthesis of the **NG-C_{60}** hybrid, comprehensive characterization was carried out using a range of physico–chemical techniques, including UV-vis absorption and fluorescence spectroscopy, FT-IR, Raman spectroscopy, X-ray photoelectron spectroscopy (XPS), and electrochemical analysis. The potential of the hybrid to undergo excited-state electron transfer

[a]*Universidad de Castilla-La Mancha, Instituto de Nanociencia, Nanotecnología y Materiales Moleculares (INAMOL), 45071-Toledo, Spain. E-mail: Fernando.Langa@uclm.es*

[b]*Chemistry and Materials Science and Engineering, University of North Texas, 76203-5017 Denton, TX, USA. E-mail: francis.dsouza@unt.edu*

[c]*Department of Physical Sciences and Mathematics, Wayne State College, 1111 Main Street, Wayne, Nebraska 68787, USA*

was subsequently investigated through density functional theory (DFT) and time-dependent DFT (TD-DFT) calculations. Finally, femtosecond transient absorption spectroscopy provided direct evidence of photoinduced charge transfer, revealing the formation of a charge-separated state with broad spatial and temporal characteristics. The key findings of this work are detailed in the following sections.

Results and discussion

The synthetic route for the preparation of the target material, **NG-C_{60}**, is outlined in Scheme 1. Previously, the fulleropyrrolidine derivative **3** was obtained in moderate yield (45%) by 1,3-dipolar cycloaddition reaction between *N*-(3,5-didodecyloxybenzyl) glycine **1** [29] and 4-((trimethylsilyl)ethynyl)benzaldehyde **2** [30] (see Experimental section in SI for further details), following the procedure reported by Prato *et al.*[31] To enhance the solubility of the fullerene derivative, dodecyloxy chains were incorporated. Compound **3** was characterized using standard spectroscopic techniques (see Fig. S1–S3 in SI). The typical pyrrolidine fingerprint appears in the ^{1}H-NMR spectrum between 5.19 and 4.17 ppm, along with the TMS signal from the protected triple bond (0.24 ppm). The structure of **3** was unequivocally confirmed by MALDI-TOF-MS spectrometry (see Fig. S3).

Next, commercial nitrogen-doped graphene, **NG** (http://www.timesnano.com), was first exfoliated using *N*-methyl-2-pyrrolidone (NMP);[32] this resulted in a dispersion of few-layer graphene sheets (3 or 4 layers) (see Fig. S4a–c). The Raman spectrum (laser 532 nm) of exfoliated NG displays the characteristic D and G bands for graphitic materials at 1353 and 1586 cm^{-1} respectively (Fig. S4a). As previously noted for nitrogen-doped graphene,[37] the presence of significant defects due to nitrogen within the graphitic network increased the intensity of the D band and broadened the Raman bands. Also, atomic force microscopy (AFM) analysis revealed that the material exhibits an average thickness of approximately 3 nm. Additionally, thinner nanosheets with an average height of ~1.4 nm, corresponding to single-layer graphene, were also identified (Fig. S4b). Finally, transmission electron microscopy (TEM) further confirmed the presence of agglomerated few-layer graphene domains, displaying lateral dimensions of several hundred nanometers and high crystallinity (Fig. S4c).

The reaction of exfoliated **NG** with 1-azido-4-(bromomethyl) benzene **4** [33] in NMP, in the presence of potassium carbonate (K_2CO_3) yielded the functionalized **NG-N_3** (see further details in SI); the triple bond of fullerene derivative **3** was deprotected with *tetra-n*-butylammonium fluoride (TBAF), followed by its reaction with **NG-N_3** in NMP *via* copper-catalysed alkyne–azide cycloaddition (click chemistry).[12,20,34,35] This process afforded the target donor–acceptor hybrid material **NG-C_{60} (5)**.

Various techniques were employed to investigate the structural and thermal properties of the new **NG**-fullerene hybrid. Thermogravimetric analysis (TGA) of the starting **NG** material showed a weight loss of approximately 10.3%, attributed to intrinsic defects; on the other hand, **NG-N_3** exhibited a gradual decrease in weight of 32.5%, a higher value attributed to the covalent incorporation of the azide group. After the "click" reaction, the hybrid material **5** showed an additional weight loss of 9.6% (after subtracting the 32.5% loss from the **NG-N3** precursor), which is attributed to the decomposition of the fulleropyrrolidine unit **3** (Fig. S5).

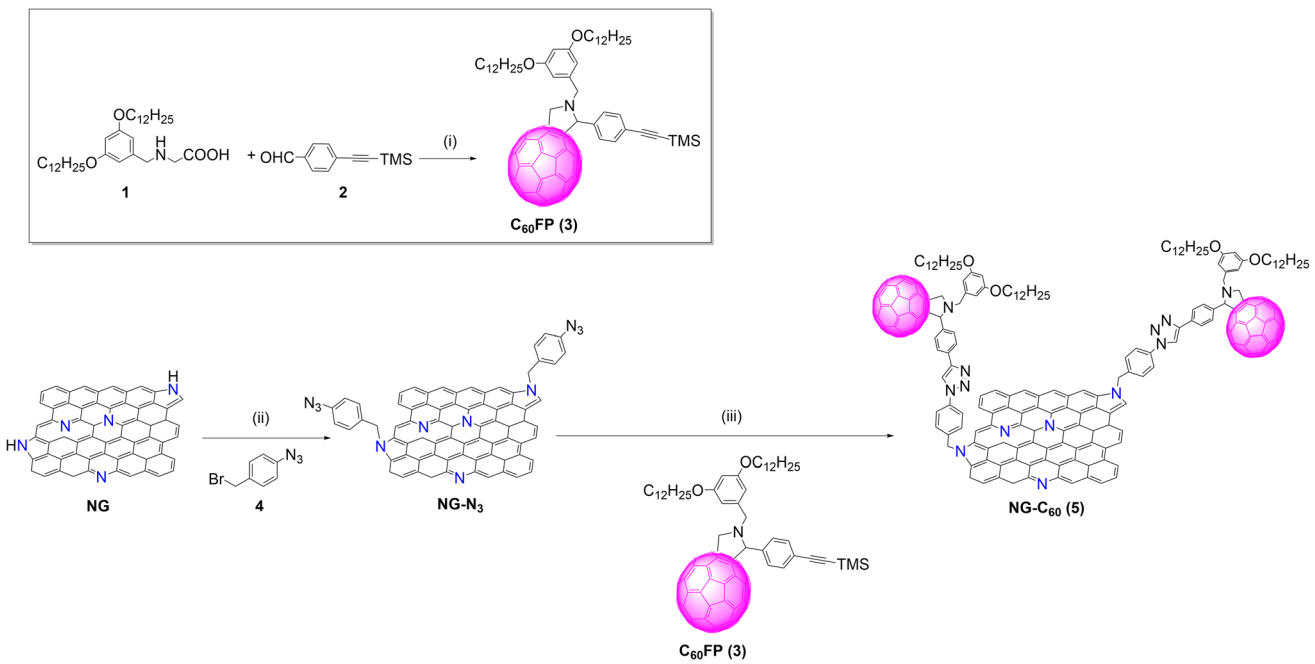

Scheme 1 Synthetic route for the preparation of **NG-C_{60} (5)** hybrid. Reagents and conditions: (i) C_{60}, toluene, 6 h, reflux, 45%; (ii) K_2CO_3, NMP, 70 °C, 48 h, (iii) TBAF, THF, NMP, rt or 0 °C, 3 h; then, $CuSO_4 \cdot 5H_2O$, sodium ascorbate, NMP, 70 °C, 48 h.

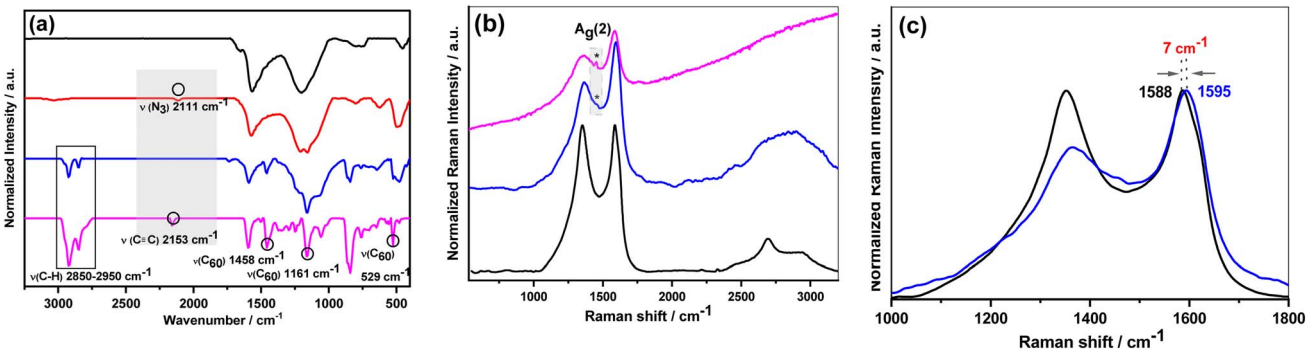

Fig. 1 (a) FTIR spectra of **NG-C$_{60}$ (5)** (—) compared with the corresponding spectra of **NG** (—), **NG-N$_3$** (—), and **3** (—). The coloured area highlights the typical region for $\nu(N_3)$ and ν(alkyne) vibrations; (b) Superimposed Raman spectra (514 nm) for (b) starting **NG** (—), **5** (—) and **3** (—); (c) Expanded G band region for **NG** (—) and functionalized **NG-C$_{60}$ (5)** (—). The spectra are normalized to the intensity of the G-mode to facilitate observation of the peak shift (7 cm^{-1}).

The FT-IR spectrum of **NG-C$_{60}$ (5)** (Fig. 1a) displays the aliphatic C–H stretching modes between 2850 and 2950 cm^{-1} (from the alkyl chains), along with the characteristic vibrational peak of C_{60} at 529 cm^{-1}, confirming effective covalent functionalization of the N-doped graphene. Additionally, the bands associated with the alkyne group in **3** and the azide moiety in **NG-N$_3$** disappeared, further verifying the success of the functionalization.[20,36]

The Raman spectrum of **NG-C$_{60}$ (5)** is shown in Fig. 1b, alongside the spectra of the starting NG material and derivative **3**. The spectrum of **5** displays the two most intense peaks typical for carbon materials: the D band (1348 cm^{-1}) and the G band (1590 cm^{-1}) bands. Evidence for the presence of the C_{60} cage is provided by the emergence of a Raman mode at 1456 cm^{-1}, assigned to the C_{60} Ag (2) pentagonal pinch mode, which is red-shifted by 4 cm^{-1} compared to that of fulleropyrrolidine precursor.[7,20,27] Furthermore, the G band in **5** is upshifted by 7 cm^{-1} relative to **NG** (Fig. 1c), attributed to the *p*-doping effect of C_{60}, consistent with previous reports on similar fullerene-containing hybrids.[7,20,27] Finally, deformation of the 2D band was also observed, likely caused by nitrogen atom intercalation.[27,37] It is important to emphasize that the hybrid material investigated in this study is nitrogen-doped graphene, and therefore not composed exclusively of carbon atoms. The incorporation of nitrogen modifies both the atomic structure and the electronic properties of the material, rendering conventional methods for estimating the degree of functionalization inapplicable. Likewise, the I_D/I_G ratio obtained from Raman spectroscopy (*vide infra*) cannot be reliably used as an indicator of functionalization, due to defect-induced band broadening associated with nitrogen doping.

X-ray photoelectron spectroscopy (XPS) analysis of **NG**, **3**, and **5** was performed (Tables S1, S2 and Fig. S6–S8). The high-resolution N 1s XPS spectrum of the starting **NG** material shows three distinct components located at 398.2, 400.2 and 401.8 eV, corresponding to pyridinic-*N*, pyrrolic-*N*, and quaternary (or "graphitic) nitrogen atoms, respectively[27] (see Fig. S6b in the SI). After the first functionalization, the N 1s spectrum of **NG-N$_3$** revealed two additional bands at binding energies of 401.5 and 404.4 eV (Fig. S7b), which are reasonably attributed to the differently charged nitrogen atoms in the azide groups.[38] Finally, XPS analysis of the C 1s and N 1s core regions of the final **NG-C$_{60}$ (5)** material (Fig. 2 and Table S1) provided definitive proof that the click reaction had occurred: (1) no peak corresponding to the free azide group at 405 eV was observed in N 1s XPS region, confirming the formation of the triazole

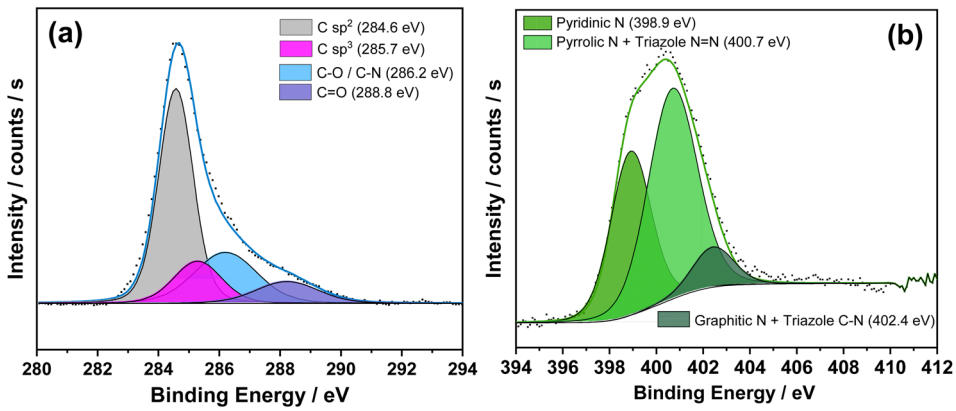

Fig. 2 (a) C 1s and (b) N 1s core level XPS regions of **NG-C$_{60}$ (5)** and their relative fits.

Table 1 Redox potentials (V *vs.* $Ag/AgNO_3$) for the investigated materials **5** and its precursor **3**, determined by OSWV[a]

Sample	E_{red}^1/V	E_{red}^2/V	E_{red}^3/V	E_{red}^4/V
3	−1.14	−1.55	−2.09	−2.55
NG-C_{60} (5)	−1.23	−1.63	−2.14	−2.54

[a] *o*-DCB/ACN solution containing 0.1 M $TBAPF_6$ and using $Ag/AgNO_3$ as a reference electrode, glassy carbon as a working electrode, and a Pt wire counter electrode. Scan rate: 100 mV s^{-1}. Potentials are referenced to Fc/Fc^+.

ring; (2) the presence of sp^3 carbon atoms (285.7 eV) from the alkyl chains of the fullerene derivative **3** was detected in the C 1s region, consistent with previous works.[28]

All these data agree with the FTIR results discussed above, confirming the successful formation of material **5** *via* click chemistry.

To further characterize the newly prepared hybrid **5**, electrochemical redox potentials were investigated by Osteryoung Square Wave Voltammetry (OSWV) in *o*-dichlorobenzene/acetonitrile (*o*-DCB/AcCN, 4 : 1 v/v) containing 0.1 M *tetra-n*-butylammonium hexafluorophosphate ($TBAPF_6$) under an argon atmosphere and at room temperature (Table 1). The **NG-C_{60} (5)** hybrid exhibits redox activity in the cathodic region, attributed to the reduction of the attached fullerene derivative. It displays the characteristic peaks of C_{60} cage at −1.23, −1.63, −2.14 and −2.54 V (Table 1 and Fig. S9). These peaks are broader and shifted by 50–90 mV compared to those of fulleropyrrolidine precursor **3** (−1.14, −1.55, −2.09 and −2.55 V respectively). These shifts are attributed to electronic interactions between the **NG** surface and the fullerene cage.[7,27]

The spectral properties of these materials were also investigated. The UV-vis absorption spectra of the pristine **NG** material revealed broad absorption across the entire spectral range, with a lower energy shoulder at 328 nm; upon attachment of the fullerene derivative, a new broad band appeared with a maximum at 429 nm, which is blue-shifted (∼5 nm) compared to the characteristic absorption peak of the precursor fullerene derivative **3** (433 nm) (Fig. 3a). Similarly, in the emission spectra, precursor fulleropyrrolidine **3** displays a weak emission band at 711 nm upon excitation at 433 nm. This band is markedly quenched in N-graphene-fullerene hybrid **5** (Fig. 3b), suggesting the occurrence of excited-state processes such as electron transfer or energy transfer.[7,20,27]

DFT and TD-DFT studies

DFT and time-dependent DFT studies play a significant role in establishing the geometry, electronic structure, and excited state properties of hybrid systems composed of donor and acceptor entities. In the present study, the **NG-C_{60}** structure was built on a local pc using GaussView 6.0. The structure was then uploaded to a supercomputer and optimized to a stationary point on the Born-Oppenheimer surface in solution at the CAM-B3LYP/6-311G(d,p) level utilizing the Self-Consistent Reaction Field (SCRF) Polarizable Continuum Model (PCM) with *o*-dichlorobenzene (κ = 9.9949) as parametrized in the Gaussian 16 software suite. The coordinates of the optimized structure are given in Table S3 in the SI. For this purpose, a reasonably large **NG** with *N*-atoms embedded in the graphene structure and functionalized through the terminal five-membered ring containing a doped N (the most reactive site for chemical functionalization) is utilized. Fig. 4 shows the optimized structure, frontier HOMO and LUMO orbitals (Fig. 4a–c). The doped N to the center of C_{60} was about 16.7 Å, revealing a lack of geometrical crowding. However, due to limited solubility, they likely exist in some aggregated form, as discussed earlier from optical studies. Notably, the HOMO on **NG** and LUMO on C_{60}, establishing their role of electron donor and electron acceptor, was borne out. This could also be envisioned from the ground-state molecular electrostatic potential map (MEP, see Fig. 4d). This trend persisted when a second C_{60} unit on the **NG** was added. Further, time-dependent DFT (TD-DFT) studies were performed for the first 25 excited states. The excitation energies ranged between 1.48 and 2.97 eV, most revealing positive oscillator strength values. The computed spectrum is bathoscopic from ∼420 to ∼840 nm. However, of the twenty-five computed excitations, only two indicate charge transfer. The calculated charge transfer band is at ∼490 nm. The band is comprised of two absorptions. A weak absorption at ∼493 nm

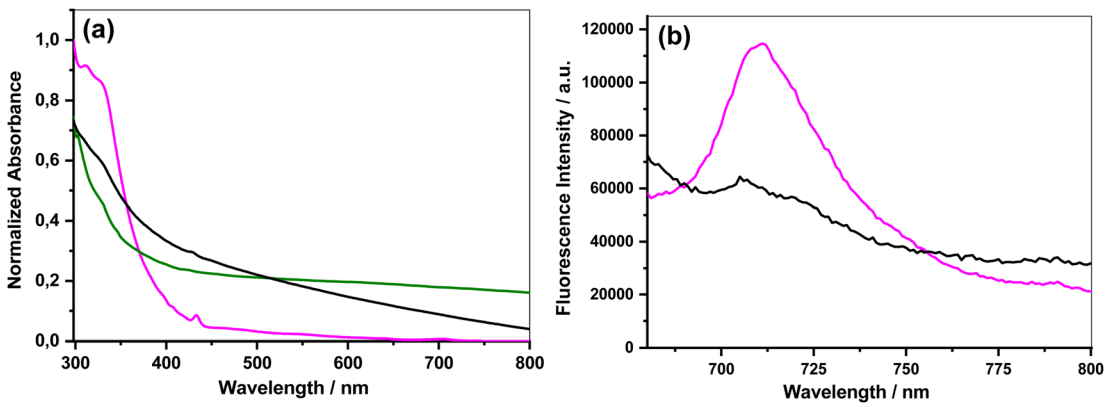

Fig. 3 (a) UV-Visible spectra of **NG-C_{60} (5)** hybrid material (—) compared to **NG** (—) and derivative **3** (—) recorded in *o*-DCB. (b) Fluorescence spectra of **NG-C_{60} (5)** hybrid material () compared to that of **3** (—) in *o*-DCB as solvent, upon excitation at 433 nm.

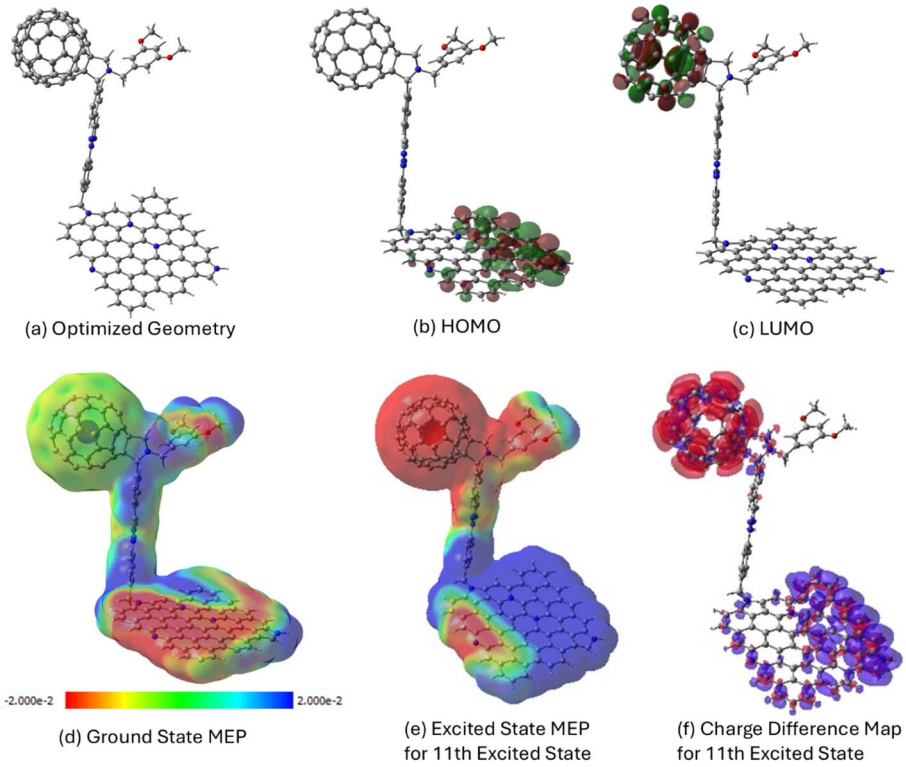

Fig. 4 (a) Optimized geometry, (b) HOMO, (c) LUMO, (d) ground state MEP, (e) first excited state MEP, and (f) charge difference map for the first excited state of **NG-C_{60}** hybrid calculated at the CAM-B3LYP/6-311G(d,p) level with the SCRF-PCM solvation model in *o*-dichlorobenzene.

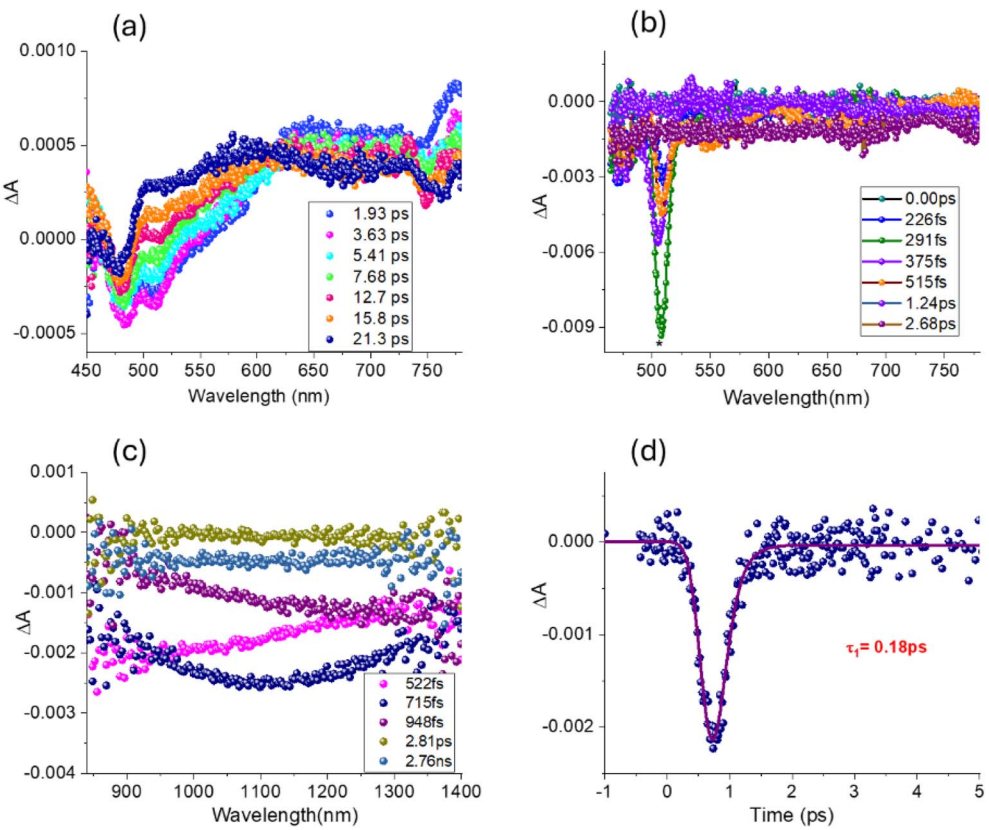

Fig. 5 Fs-TA spectra at the indicated delay times of C_{60} used in the click reaction, (b and c) of **NG** covering the visible and near-IR region, and (d) the **NG** exciton time profile. The samples were excited using a 100-fs pulsed laser tuned to 433 nm for C_{60} and 440 nm for **NG** in DMF.

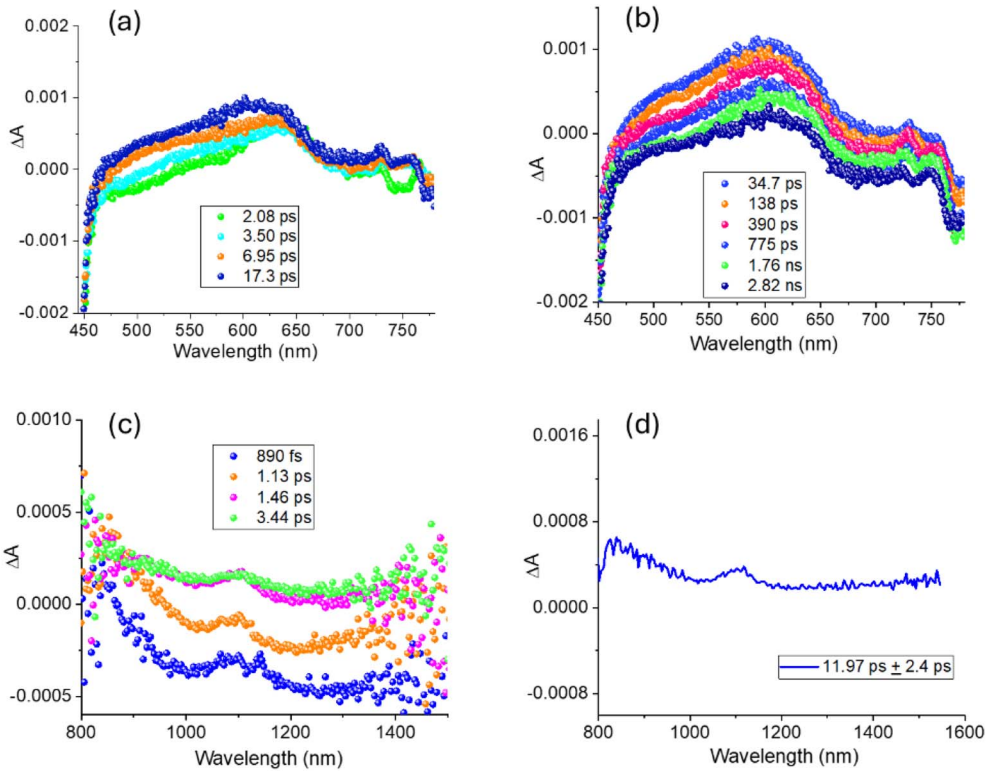

Fig. 6 Fs-TA spectra at the indicated delay times of the **NG-C_{60}** hybrid (a and b covering the visible region and c covering the near-IR region). The result of global target analysis is shown in Fig. 6d. The sample was excited using a 100-fs pulsed laser tuned to 433 nm, corresponding to C_{60} in DMF.

(2.52 eV), which is the 11th excited state (HOMO-3 → LUMO+1). A strong absorption at ~490 nm (2.53 eV), which is the 13th excited state (HOMO-2 → LUMO+3). The charge difference maps from the ground state to the assigned one, and the excited state MEPs are shown in Fig. 4e and f for the first excited state, while Fig. S10 and S11 in the SI show the first six excited states. Clear segregation of charges on the fullerene (negative charge) and **NG** (positive charge) parts was witnessed for the first five excited states (the 6th is a locally excited state), indicating the occurrence of excited-state charge separation in this hybrid.

Femtosecond transient absorption studies

Encouraged by these theoretical predictions, femtosecond transient absorption (fs-TA) spectral studies were performed in DMF by exciting the samples at 440 nm to seek evidence of excited-state charge separation in this hybrid. First, the fs-TA spectra of the C_{60} derivative used in the click reaction were investigated. As shown in Fig. 5a, the instantaneously formed $^1C_{60}$* revealed excited state absorption (ESA) peaks in the 640–720 nm range, and at 772 nm. Weaker ground state bleaching (GSB) peaks at 483 and 511 nm, and a stimulated emission (SE) type peak at 745 nm was observed. Decay and recovery of the ESA and GSB/SE peaks revealed a new broad peak in the 550–650 nm range corresponding to $^3C_{60}$*, a product of intersystem crossing (ISC). The fs-TA spectra of pristine NG shown in Fig. 5b revealed no measurable signal (the sharp peak at 510 nm is due to instrument scattering); however, in the near-IR region, weak transient features corresponding to an exciton were observed (Fig. 5c). Kinetic analysis of this signal (Fig. 5d) resulted in a lifetime of 0.18 ps, which agreed with the earlier reported value. The photo response of both NG and C_{60} used in building the donor–acceptor hybrid is borne out by this study.

Fig. 6a and b show the fs-TA spectra at the indicated delay times for **NG-C_{60}** in DMF. At earlier delay times, the spectral features were what was observed for the C_{60} control in Fig. 5a. That is, the formation of $^1C_{60}$* and later, undergoing ISC to populate $^3C_{60}$*. Interestingly, in the near-IR region, the excitonic peak of **NG** also had a clear peak in the 1000 nm region (see spectrum at 890 fs in Fig. 6c), expected for C_{60}^- that lasted beyond the excitonic peak recovery time (see spectrum at 3.44 ps in Fig. 6c), indicating charge transfer in the **NG-C_{60}** hybrid. The broad nature of this peak could be attributed to the low solubility (aggregation) of the hybrid. Global data analysis was subsequently performed, which resulted in a lifetime of ~12 ps for the charge transfer state (see Fig. 6d). These results provide clear evidence that NG-$^1C_{60}$* undergoes a charge transfer state and subsequently populates the $^3C_{60}$* before returning to the ground state, as evidenced by the data in Fig. 6b.

Summary and conclusions

In this study, we successfully synthesized a novel donor–acceptor hybrid material composed of nitrogen-doped graphene (**NG**) covalently linked to a fullerene (C_{60}) derivative *via* copper-

catalyzed azide–alkyne cycloaddition (click chemistry). This synthetic strategy enabled a higher degree of functionalization, improved reaction yields, and reduced reaction times compared to previously reported methods. The resulting **NG-C_{60}** hybrid exhibited good solubility in organic solvents, facilitating comprehensive structural and spectroscopic characterization.

Theoretical investigations using DFT and TD-DFT calculations supported the formation of a charge-separated state, with the HOMO localized on the **NG** donor and the LUMO on the C_{60} acceptor. These predictions were experimentally validated by femtosecond transient absorption spectroscopy, which revealed ultrafast charge separation and the formation of a charge transfer state with a lifetime of approximately 12 ps, followed by population of the triplet C_{60}* state.

Overall, the **NG-C_{60}** hybrid developed in this work represents a promising platform for light-harvesting applications, offering a robust and tunable architecture for efficient photoinduced charge separation. These findings contribute to the broader development of carbon-based donor–acceptor systems for energy conversion technologies.

Author contributions

All the authors approved the final version of the manuscript.

Conflicts of interest

The authors declare no conflicts of interest.

Data availability

The data supporting the findings of this study are included in the main text and in the supplementary information (SI). Additionally, they are available from the corresponding author upon reasonable request. The data have also been deposited in Zenodo and can be accessed *via* the following link: **https://zenodo.org/records/17293193**. See DOI: **https://doi.org/10.1039/d5sc06142c**.

Acknowledgements

This work was financially supported by MICINN of Spain (PID2022-141687OB-I00 and TED2021-131255B-C42) and the Junta de Comunidades de Castilla-La Mancha, together with European FEDER funds (SBPLY/21/180501/000142) and by the US-National Science Foundation (2345836 to FD). M. A. thanks MINECO (CTQ2016-79189-R) for a doctoral FPI grant.

References

1 D. Gust, T. A. Moore and A. L. Moore, *Acc. Chem. Res.*, 2009, **42**, 1890.
2 F. D'Souza and O. Ito, *Chem. Soc. Rev.*, 2012, **41**, 86.
3 M. R. Wasielewski, *Chem. Rev.*, 1992, **92**, 435.
4 G. B. Daniel, K. Nachimuthu and J. L. Nallasivam, *Chem Asian J.*, 2025, **20**, e202401800.
5 M. Barrejón, L. M. Arellano, F. D'Souza and F. Langa, *Nanoscale*, 2019, **11**, 14978.
6 M. Vizuete, M. Barrejón, M. J. Gómez-Escalonilla and F. Langa, *Nanoscale*, 2012, **4**, 4370.
7 M. Barrejón, H. B. Gobeze, M. J. Gómez-Escalonilla, J. L. G. Fierro, M. Zhang, M. Yudasaka, S. Iijima, F. D'Souza and F. Langa, *Nanoscale*, 2016, **8**, 14716.
8 T. Umeyama and H. Imahori, *J. Phys. Chem. C*, 2013, **117**, 3195.
9 T. Umeyama and H. Imahori, *Nanoscale Horiz.*, 2018, **3**, 352.
10 M. Chen, R. Guan and S. Yang, *Adv. Sci.*, 2019, **6**, 1800941.
11 M. Vizuete, M. J. Gómez-Escalonilla, J. L. G. Fierro, K. Ohkubo, S. Fukuzumi, M. Yudasaka, S. Iijima, J. F. Nierengarten and F. Langa, *Chem. Sci.*, 2014, **5**, 2072.
12 M. Vizuete, M. J. Gómez-Escalonilla, J. L. G. Fierro, M. Yudasaka, S. Iijima, M. Vartanian, J. Iehl, J.-F. Nierengarten and F. Langa, *Chem. Commun.*, 2011, **47**, 12771.
13 G. Bottari, M. Á. Herranz, L. Wibmer, M. Volland, L. Rodríguez-Pérez, D. M. Guldi, A. Hirsch, N. Martín, F. D'Souza and T. Torres, *Chem. Soc. Rev.*, 2017, **46**, 4464.
14 K. Jayaramulu, S. Mukherjee, D. M. Morales, D. P. Dubal, A. K. Nanjundan, A. Schneemann, J. Masa, S. Kment, W. Schuhmann, M. Otyepka, R. Zbořil and R. A. Fischer, *Chem. Rev.*, 2022, **122**, 17241.
15 A. Criado, M. Melchionna, S. Marchesan and M. Prato, *Angew. Chem., Int. Ed.*, 2015, **54**, 10734.
16 Z. Li, Z. Liu, H. Sun and C. Gao, *Chem. Rev.*, 2015, **115**, 7046.
17 M. Barrejón, M. J. Gómez-Escalonilla, J. L. G. Fierro, P. Prieto, J. R. Carrillo, A. M. Rodríguez, G. Abellán, M. C. López-Escalante, M. Gabás, J. T. López-Navarrete and F. Langa, *Phys. Chem. Chem. Phys.*, 2016, **18**, 29582.
18 A. Stergiou, R. Cantón-Vitoria, M. N. Psarrou, S. P. Economopoulos and N. Tagmatarchis, *Prog. Mater. Sci.*, 2020, **114**, 100683.
19 R. Canton-Vitoria, A. Z. Alsaleh, G. Rotas, Y. Nakanishi, H. Shinohara, F. D' Souza and N. Tagmatarchis, *Nanoscale*, 2022, **14**, 15060.
20 M. Barrejón, M. Vizuete, M. J. Gómez-Escalonilla, J. L. G. Fierro, I. Berlanga, F. Zamora, G. Abellán, P. Atienzar, J.-F. Nierengarten, H. García and F. Langa, *Chem. Commun.*, 2014, **50**, 9053.
21 H. Xu, L. Ma and Z. Jin, *J. Energy Chem.*, 2018, **27**, 146.
22 R. Yadav and C. K. Dixit, *J. Sci. Adv. Mater. Devices*, 2017, **2**, 141.
23 P. Lazar, R. Mach and M. Otyepka, *J. Phys. Chem. C*, 2019, **123**, 10695.
24 H. Wang, T. Maiyalagan and X. Wang, *ACS Catal.*, 2012, **2**, 781.
25 C. Hu, D. Liu, Y. Xiao and L. Dai, *Prog. Nat. Sci.*, 2018, **28**, 121.
26 M. Barrejón, A. Primo, M. J. Gómez-Escalonilla, J. L. G. Fierro, H. García and F. Langa, *Chem. Commun.*, 2015, **51**, 16916.
27 M. Barrejón, L. M. Arellano, H. B. Gobeze, M. J. Gómez-Escalonilla, J. L. G. Fierro, F. D'Souza and F. Langa, *Chem. Sci.*, 2018, **9**, 8221.

28 L. M. Arellano, H. B. Gobeze, Y. Jang, M. Barrejón, C. Parejo, J. C. Álvarez, M. J. Gómez-Escalonilla, Á. Sastre-Santos, F. D'Souza and F. Langa, *Chem.–Eur. J.*, 2022, **28**, e202200254.
29 F. Ajamaa, T. M. Figueira Duarte, C. Bourgogne, M. Holler, P. W. Fowler and J.-F. Nierengarten, *Eur. J. Org Chem.*, 2005, 3766.
30 F. Auras, L. Ascherl, A. H. Hakimioun, J. T. Margraf, F. C. Hanusch, S. Reuter, D. Bessinger, M. Döblinger, C. Hettstedt, K. Karaghiosoff, S. Herbert, P. Knochel, T. Clark and T. Bein, *J. Am. Chem. Soc.*, 2016, **138**, 16703.
31 M. Prato and M. Maggini, *Acc. Chem. Res.*, 1998, **31**, 519.
32 H. B. Gobeze, L. M. Arellano, A. M. Gutiérrez-Vílchez, M. J. Gómez-Escalonilla, Á. Sastre-Santos, F. Fernández-Lázaro, F. Langa and F. D'Souza, *Nanoscale Adv.*, 2019, **1**, 4009.
33 M. Belkheira, D. El Abed, J.-M. Pons and C. Bressy, *Chem.–Eur. J.*, 2011, **17**, 12917.
34 M. Vizuete, M. J. Gómez-Escalonilla, J. L. G. Fierro, A. S. D. Sandanayaka, T. Hasobe, M. Yudasaka, S. Iijima, O. Ito and F. Langa, *Chem.–Eur. J.*, 2010, **16**, 10752.
35 J. Mateos-Gil, L. Rodríguez-Pérez, M. Moreno Oliva, G. Katsukis, C. Romero-Nieto, M. Á. Herranz, D. M. Guldi and N. Martín, *Nanoscale*, 2015, **7**, 1193.
36 L. Rodríguez-Pérez, J. Ramos-Soriano, A. Pérez-Sánchez, B. M. Illescas, A. Muñoz, J. Luczkowiak, F. Lasala, J. Rojo, R. Delgado and N. Martín, *J. Am. Chem. Soc.*, 2018, **140**, 9891.
37 N. Mahmood, C. Zhang, H. Yin and Y. Hou, *J. Mater. Chem. A*, 2014, **2**, 15.
38 G. Tuci, D. Mosconi, A. Rossin, L. Luconi, S. Agnoli, M. Righetto, C. Pham-Huu, H. Ba, S. Cicchi, G. Granozzi and G. Giambastiani, *Chem. Mater.*, 2018, **30**, 8257.